To appear in The Astrophysical Journal
Preprint typeset using LaTeX style emulateapj v. 04/17/13

arXiv:1403.1207v1 [astro-ph.GA] 5 Mar 2014

WIDESPREAD ROTATIONALLY-HOT HYDRONIUM ION IN THE GALACTIC INTERSTELLAR MEDIUM

D. C. Lis[1,2], P. Schilke[3], E. A. Bergin[4], M. Gerin[5], J. H. Black[6], C. Comito[3], M. De Luca[5], B. Godard[5], R. Higgins[3], F. Le Petit[5], J. C. Pearson[7], E. W. Pellegrini[8], T. G. Phillips[1], and S. Yu[7]

(Received 2014 January 16; Accepted 2014 March 4)
To appear in The Astrophysical Journal

ABSTRACT

We present new *Herschel*[a] observations of the (6,6)[b] and (9,9) inversion transitions of the hydronium ion toward Sagittarius B2(N) and W31C. Sensitive observations toward Sagittarius B2(N) show that the high, ∼500 K, rotational temperatures characterizing the population of the highly-excited metastable H_3O^+ rotational levels are present over a wide range of velocities corresponding to the Sagittarius B2 envelope, as well as the foreground gas clouds between the Sun and the source. Observations of the same lines toward W31C, a line of sight that does not intersect the Central Molecular Zone, but instead traces quiescent gas in the Galactic disk, also imply a high rotational temperature of ∼380 K, well in excess of the kinetic temperature of the diffuse Galactic interstellar medium. While it is plausible that some fraction of the molecular gas may be heated to such high temperatures in the active environment of the Galactic center, characterized by high X-ray and cosmic ray fluxes, shocks and high degree of turbulence, this is unlikely in the largely quiescent environment of the Galactic disk clouds. We suggest instead that the highly-excited states of the hydronium ion are populated mainly by exoergic chemical formation processes and temperature describing the rotational level population does not represent the physical temperature of the medium. The same arguments may be applicable to other symmetric top rotors, such as ammonia. This offers a simple explanation to the long-standing puzzle of the presence of a pervasive, hot molecular gas component in the central region of the Milky Way. Moreover, our observations suggest that this is a universal process, not limited to the active environments associated with galactic nuclei.

Keywords: astrochemistry — galaxies: nuclei — ISM: molecules — molecular processes — submillimeter — techniques: spectroscopic

1. INTRODUCTION

The presence of molecules in interstellar space was predicted as early as 1930's (e.g., Swings & Rosenfeld 1937), quickly followed by identification of simple diatomic species, CH, CN, CH^+ (e.g., McKellar 1940), in optical absorption spectra. These early observations lead to important insights into the physics and chemistry of the interstellar medium (e.g., Bates & Spitzer 1951). However, the optical and UV observations are limited to diffuse or translucent clouds and applications of molecular spectroscopy to studies of the dense interstellar medium had to await the development of microwave detection techniques in the 1960s. Since the first microwave detections of molecules in space (Weinreb et al. 1963; Cheung et al. 1969; Wilson et al. 1970), molecular spectroscopy has been a premier tool for studying interstellar gas cloud physics, from the Milky Way (Evans 1999) to the high-redshift universe (Solomon & Vanden Bout 2005). In order to use molecules as quantitative tracers of star-forming clouds, it is necessary to understand the radiative and collisional processes that govern the excitation of their internal quantum states (Flower 2007). For decades, it has been theorized that, under interstellar conditions, some molecules form via highly-exothermic reactions between ions and neutral molecules (Herbst & Klemperer 1973). However, quantitative models of chemistry and of excitation have conventionally been constructed independently, on the grounds that chemical time-scales are long compared with excitation time-scales.

The most abundant interstellar molecule, molecular hydrogen, is a symmetric rotor without a permanent dipole moment, which only has weak quadrupole rovibrational transitions in its ground electronic state (e.g., Habart et al. 2005). Its UV electronic transitions can only be studied from space and the observations are

[1] California Institute of Technology, Cahill Center for Astronomy and Astrophysics 301-17, Pasadena, CA 91125, USA; dcl@caltech.edu, tgp@submm.caltech.edu
[2] Sorbonne Universités, Université Pierre et Marie Curie, Paris 6, CNRS, Observatoire de Paris, UMR 8112, LERMA, Paris, France
[3] I. Physikalisches Institut, University of Cologne, Zülpicher Str. 77, 50937 Köln, Germany; schilke@ph1.uni-koeln.de, ccomito@ph1.uni-koeln.de, higgins@ph1.uni-koeln.de
[4] University of Michigan, Ann Arbor, Michigan 48109, USA; ebergin@umich.edu
[5] École Normale Superiéure, CNRS, Observatoire de Paris, UMR 8112, LERMA, Paris, France; maryvonne.gerin@lra.ens.fr, deluca@lra.ens.fr, benjamin.godard@lra.ens.fr, franck.lepetit@obspm.fr
[6] Department of Earth and Space Sciences, Chalmers University of Technology, Onsala Space Observatory, SE-43992 Onsala, Sweden; john.black@chalmers.se
[7] Jet Propulsion Laboratory, California Institute of Technology, 4800 Oak Grove Drive, Pasadena, CA 91109, USA; john.c.pearson@jpl.nasa.gov, shanshan.yu@jpl.nasa.gov
[8] Department of Physics and Astronomy, University of Toledo, Toledo, OH 43606, USA; eric.pellegrini@utoledo.edu

[a] Herschel is an ESA space observatory with science instruments provided by European-led Principal Investigator consortia and with important participation from NASA.

[b] The correct spectroscopic notation should be $J_K = 6_6^- \leftarrow 6_6^+$, but we follow here the notation commonly used in the ammonia literature.

limited to the relatively nearby diffuse and translucent clouds. The infrared rovibrational lines are accessible from the ground, but are only excited in warm, active environments, such as shocks or photon dominated regions. Consequently, trace molecules, with rich rotational spectra in the millimeter to far-infrared wavelength range have been used as proxies of H_2, to understand the physical conditions in the star-forming gas reservoir of the Milky Way and external galaxies. Of these, oblate symmetric top molecules, in particular ammonia (Ho & Townes 1983), for which the $J = K$ level is the lowest energy level in each K ladder, are of great utility for the temperature determination. The population of these "metastable" levels is assumed to be thermalized at the kinetic temperature of the medium, due to the absence of allowed radiative transitions out of these levels.

The hydronium ion, H_3O^+, is another oblate symmetric rotor, isoelectronic with ammonia, which like ammonia has the characteristic inversion splitting of its rotational levels. In the case of H_3O^+, however, the splitting is very large (Liu & Oka 1985) and the inversion transitions occur at far-infrared wavelengths, as opposed to centimeter wavelengths for ammonia. The far-infrared H_3O^+ inversion transitions, up to (11,11), have only recently been detected for the first time by *Herschel*, in absorption toward the central region of the Milky Way (Lis et al. 2012).

Earlier HIFI observations of the hydronium ion toward Sagittarius B2 indicated a high rotational temperature, ∼500 K, at velocities corresponding to the cloud envelope. Lis et al. (2012) suggested that, in regions exposed to ionizing radiation, such as those at the center of the Milky Way, highly-excited states of the hydronium ion and ammonia are populated mainly by exoergic chemical formation processes and temperatures derived from their spectra do not represent the physical temperature of the medium. The detection of highly-excited states of the hydronium ion in nearby active galaxies, with rotational temperatures similar to that observed in Sagittarius B2 (González-Alfonso et al. 2013), demonstrated the universality of the shape of the observed population diagrams in *active* environments. Here we present new sensitive *Herschel* observations of the hydronium ion on the lines of sight toward Sagittarius B2(N) and W31C (G10.6-0.4), which clearly demonstrate that this effect is not limited to the environments of galactic nuclei, characterized by high X-ray and cosmic ray fluxes, but is a *fundamental* property, pervasive throughout the interstellar medium.

2. OBSERVATIONS

The inversion lines of H_3O^+ were first discovered in absorption in the full spectral scans of Sagittarius B2(M)[9] and (N)[10] carried out between 2010 March and 2011 April using the Heterodyne Instrument for the Far-Infrared (HIFI; De Graauw et al. 2010) on the Herschel Space Observatory (Pilbratt et al. 2010), within the framework of the HEXOS guaranteed time key program (Bergin et al. 2010). Preliminary analysis of the Sagittarius B2(N) data was presented by Lis et al. (2012). The data presented here have been re-reduced using an improved version of the HIFI pipeline, which results in significantly lower noise levels in the high-frequency HEB mixer bands. The source coordinates are: Sagittarius B2(M) $\alpha_{J2000} = 17^h47^m20.35^s, \delta_{J2000} = -28°23'03.00''$; Sagittarius B2(N) $\alpha_{J2000} = 17^h47^m19.88^s, \delta_{J2000} = -28°22'18.40''$.

The line survey data have been calibrated with HIPE version 10.0 (Roelfsema et al. 2012) and the resulting double-sideband (DSB) spectra were subsequently reduced using the GILDAS CLASS[11] software package. Basic data reduction steps included removal of spurious features or otherwise unusable portions of the spectra. The continuum emission was then subtracted from the DSB scans by fitting a low-order (typically 0–1, in a few cases 2) polynomial. The continuum-subtracted DSB data were deconvolved (sideband separation through pure χ^2 minimization; Comito & Schilke 2002) to provide a single-sideband (SSB) spectrum for each HIFI band.

The variation of the continuum intensity as a function of frequency was determined from the least-squares fit to the emission-free spectral channels across all HIFI bands. The fitted continuum was subsequently folded back into the deconvolved, baseline subtracted spectra. The data reduction procedure ensures that saturated absorption features reach the zero continuum level and there are no discontinuities in the overlap regions between the various HIFI bands.

In addition to the full HIFI spectral scans, we obtained deep follow-up integrations at the frequencies of the (6,6) and (9,9) inversion transitions of the hydronium ion toward Sagittarius B2(N) and W31C. These observations[12] were carried out in 2012 October 4–17 in the framework of the special, final call for *Herschel* observing proposals, referred to by ESA as "Must-Do" programs. The source coordinates for W31C are $\alpha_{J2000} = 18^h10^m28.70^s, \delta_{J2000} = -19°55'50.00''$ and for Sagittarius B2 are the same as the earlier HEXOS observations. The data were taken in the double beam switching (DBS) mode, with the reference beams ∼180″ away from the source, using the HIFI wideband spectrometer (WBS), which provides a 1.1. MHz frequency resolution over the 2.4 GHz bandwidth of the band 7 HEB receivers. Three shifted LO settings were observed, which were subsequently averaged together after inspecting the spectra for possible line contamination from image sideband (no contamination was found). The total observing time for each of the two sources was 53 and 56 min for the (6,6) and (9,9) lines, respectively.

Spectra from the HIFI HEB mixer bands are known to be adversely affected by standing waves originating in the signal amplification chain. This problem is particularly apparent in long integrations, such as the deep Sagittarius B2(N) and W31C observations presented here, where the detector power levels can drift significantly, resulting

[9] *Herschel* OBSIDs: 1342191565, 2546, 2656, 1342204723, 4739, 5848, 6455, 6501, 664, 1342215935, 6702, and 8200; OD 292–693.

[10] *Herschel* OBSIDs: 1342204692, 4703, 4731, 4812, 4829, 5491, 5855, 6364, 6370, 6498, 6643, 1342215934, 6701, and 8198; OD 489–693.

[11] http://www.iram.fr/IRAMFR/GILDAS

[12] *Herschel* OBSIDs: 1342252167–169, 174–176, 134253608, 610–12; OD 1239 and 1252.

in a disparity between the "on" and "off" phases of the observation. Since the standing waves occur in the electrical chain, where the reflecting components have complex frequency-dependent impedance, the resulting baseline ripple has a non-sinusoidal behavior and it is difficult to remove using standard standing wave removal techniques (Higgins & Kooi 2009). Fortunately the standing wave phase and amplitude are stable for a given mismatch between the "on" and "off" phases. Therefore, the spectra can be corrected by subtracting a standing wave profile from similarly mismatched template spectra. This approach has been applied here to the individual integrations, before they were averaged together to produce the final spectra.

3. SAGITTARIUS B2 RESULTS

Continuum-divided spectra of the H_3O^+ inversion lines toward Sagittarius B2(M) and (N) from the HEXOS spectral scans are shown in Figure 1, upper and lower panels, respectively. The lower panel is a revised version of Figure 3 of Lis et al. (2012), including latest improvements in the data processing. The (1,1) line is not included in the analysis, as it is blended with the strong $2_{12} - 1_{01}$ line of $H_2^{18}O$. Instead, the $J_K = 0_0^- \leftarrow 1_0^+$ ground state ortho-H_3O^+ spectrum is included (see energy level diagram in Figure 2 of Lis et al. 2012). Gaussian fit results for the two sources are listed in Tables 1 and 2. We use the latest line frequencies of Yu & Pearson (2014), which in some cases differ by up to ∼25 MHz from those used in Lis et al. (2012). The H_3O^+ column densities in the metastable levels can be derived directly from the velocity integrated optical depths of the corresponding inversion transitions using the formula (see, e.g., eq. 3 of Neufeld et al. 2010):

$$N_l(H_3O^+) = \frac{8\pi g_l}{A_{ul} g_u \lambda^3} \int \tau dv \ ,$$

where A_{ul} is the spontaneous emission coefficient, g_u and g_l the upper and lower level degeneracies, and λ the wavelength. Spectroscopic constants for the observed transitions are included for completeness in Table 1 and the resulting rotation diagrams (plots of the logarithm of the integrated line strength as a function of the lower level energy; e.g., Linke et al. 1979) for the two sources are also shown in Figure 1. Toward Sagittarius B2(M), the spectrum is dominated by a single component centered around 64 km s^{-1}, with a line width of 15 km s^{-1}, associated with the cloud envelope. Three velocity components, centered around 5, 65, and 80 km s^{-1}, with line widths of ∼25, 19, and 11 km s^{-1} respectively, can be identified in the Sagittarius B2(N) spectra. The strongest component at 65 km s^{-1} is associated with the cloud envelope and contains ∼60% of the total H_3O^+ column density. The spectra are not sensitive enough to produce independent rotational diagrams for the individual velocity components. Therefore the three components have been added together to produce a single rotational diagram for this source.[13]

[13] There is evidence that the 5 km s^{-1} component may have a somewhat higher rotational temperature than the other two, stronger components that are responsible for the bulk of the absorption (see Fig. 2).

The rotational diagrams for the two sources naturally separate into "warm" and "hot" components (blue and red points in Figure 1; lower level energies below and above 200 K, respectively). Rotational temperatures, determined separately for the warm and hot components from the least square fits to the data, are shown in Figure 1 with the corresponding uncertainties, which should be viewed as *maximum* uncertainties due to systematics, such as baseline removal. We conservatively assume a 25% maximum uncertainty for the individual measurements.

The warm component toward the two sources is well described by a rotational temperature of ∼175 ± 50 K, while the temperatures of the hot component toward the two sources are consistent with 485 ± 65 K (maximum uncertainties). A two-component fit is only an approximation to the observed rotation diagram and a continuous range of temperatures between these limiting values is possible. However, one clear conclusion is that the population of the highest and lowest-energy metastable levels is described by *different* rotational temperatures, ∼175 and 485 K, respectively.

Total H_3O^+ column densities toward Sagittarius B2(N) and (M), obtained by adding up the population in the observed rotational levels, are 1.1×10^{15} and 4.4×10^{14} cm^{-2}, respectively, with ∼40% of the total column density in the hot component. The extended envelope of Sagittarius B2, with a velocity of ∼65 km s^{-1} has a column density of 7×10^{14} cm^{-2} on the line of sight toward Sagittarius B2(N). This is ∼50% higher than the corresponding value toward Sagittarius B2(M). This, together with the fact that the 80 km s^{-1} component that is quite prominent in the Sagittarius B2(N) spectra is not seen toward Sagittarius B2(M), suggests that significant variations in the H_3O^+ column density are present on linear scales of order 1.7 pc. If the absorption originated in a foreground shocked screen between the Sun and Sagittarius B2 (e.g., Ceccarelli et al. 2002), one would not expect such large column density variations.

The new Sagittarius B2(N) deep integrations are much more sensitive than the HEXOS spectral scans. The continuum-divided spectra of the (6,6) and (9,9) transitions are shown in Figure 2 (blue and red lines, respectively; average of the H and V polarizations, equally weighted; left vertical scale). H_3O^+ absorption is clearly detected over a wide range of LSR velocities between about –120 and +90 km s^{-1}. The (9,9) absorption at the most negative velocities is contaminated by the strong $J_K = 3_1^- \leftarrow 2_1^+$ line of ammonia in the same sideband, which may affect the derived line ratio and the corresponding rotational temperature at these velocities. It is not possible to remove the contamination, because the only other para-NH_3 line with comparable line strength and lower level energy is itself blended and the intrinsic line profile cannot be determined.

Black points in Figure 2 show the (9,9)/(6,6) optical depth ratio in 1 km s^{-1} channels (left vertical scale). Only points corresponding to velocities at which absorption in both transitions is detected above 4σ level in individual channels are plotted. The corresponding 1σ uncertainties are computed from the difference between the H and V polarization spectra, which are assumed to be independent measurements. The rotational temperature

Table 1
H_3O^+ Spectroscopic Parameters and Absorption Line Parameters toward Sagittarius B2(M)

Transition	ν_{ul}	A_{ul}	g_u	g_l	E_l	V	ΔV	τdv
(1,1)	1655.834	5.464×10^{-2}	6	6	0	—	—	—
$0_0^- - 1_0^+$	984.712	2.298×10^{-2}	4	12	7.3	64.9 ± 0.2	13.4 ± 0.5	6.10 ± 0.18
(2,2)	1657.248	7.303×10^{-2}	10	10	42.7	64.4 ± 0.4	12.9 ± 0.9	7.33 ± 0.49
(3,3)	1663.587	8.312×10^{-2}	28	28	103.1	64.6 ± 0.3	14.7 ± 0.7	16.6 ± 0.7
(4,4)	1674.866	9.047×10^{-2}	18	18	181.2	64.5 ± 0.3	15.6 ± 0.8	7.97 ± 0.36
(5,5)	1691.134	9.701×10^{-2}	22	22	276.9	64.3 ± 0.3	15.6 ± 0.7	5.83 ± 0.22
(6,6)	1712.461	1.036×10^{-1}	52	52	390.2	64.0 ± 0.4	15.7 ± 0.7	10.7 ± 0.4
(7,7)	1738.936	1.107×10^{-1}	30	30	521.1	64.1 ± 0.6	15.1 ± 1.2	4.06 ± 0.29
(8,8)	1770.679	1.188×10^{-1}	34	34	669.5	65.0 ± 0.6	17.4 ± 1.5	4.66 ± 0.33
(9,9)	1807.826	1.280×10^{-1}	76	76	835.3	64.0 ± 0.4	16.2 ± 1.0	7.50 ± 0.39
(10,10)	1850.536	1.387×10^{-1}	42	42	1019.	64.8 ± 0.5	16.8 ± 1.2	3.52 ± 0.22
(11,11)	1898.992	1.511×10^{-1}	46	46	1219.	62.9 ± 1.3	23.7 ± 3.5	1.94 ± 0.23

Note. — Entries in the table are: transition, frequency (GHz), spontaneous emission coefficient (s^{-1}), upper and lower level degeneracies, lower level energy (K), as well as the observed line center velocity, line width, and velocity integrated line opacity ($km\,s^{-1}$). The (1,1) line in the Galactic center sources is blended with the $2_{12} - 1_{01}$ transition of $H_2^{18}O$ and cannot be used in the analysis.

Table 2
H_3O^+ Absorption Line Parameters toward Sagittarius B2(N)

Transition	5 $km\,s^{-1}$		65 $km\,s^{-1}$		80 $km\,s^{-1}$		Total
	V	τdv	V	τdv	V	τdv	τdv
$0_0^- - 1_0^+$	4.4 ± 3.0	1.59 ± 0.30	66.7 ± 0.3	9.7 ± 0.3	81.9 ± 0.7	1.58 ± 0.23	12.9 ± 0.5
(2,2)	4.1 ± 1.9	3.39 ± 0.43	66.0 ± 0.4	13.0 ± 0.4	81.2 ± 0.7	2.31 ± 0.33	18.7 ± 0.7
(3,3)	6.3 ± 1.3	8.26 ± 0.63	66.0 ± 0.3	25.9 ± 0.6	80.6 ± 0.5	5.74 ± 0.53	$40. \pm 1.0$
(4,4)	7.4 ± 1.3	3.10 ± 0.25	65.7 ± 0.3	11.3 ± 0.3	80.8 ± 0.5	2.87 ± 0.21	17.2 ± 0.5
(5,5)	7.6 ± 2.0	4.36 ± 0.45	64.3 ± 0.6	9.2 ± 0.4	80.2 ± 0.7	3.37 ± 0.35	17.0 ± 0.7
(6,6)	5.6 ± 1.8	8.85 ± 0.90	64.6 ± 0.7	18.8 ± 0.9	79.8 ± 1.1	4.45 ± 0.76	$32. \pm 1.5$
(7,7)	5.4 ± 1.2	3.39 ± 0.27	66.3 ± 0.5	7.4 ± 0.3	80.9 ± 0.8	1.85 ± 0.23	12.7 ± 0.5
(8,8)	3.2 ± 2.2	2.45 ± 0.35	65.2 ± 0.8	5.9 ± 0.4	79.8 ± 1.0	1.83 ± 0.31	10.2 ± 0.6
(9,9)	5.4 ± 2.4	4.94 ± 0.75	65.4 ± 1.3	9.4 ± 0.8	79.1 ± 1.4	3.38 ± 0.74	17.8 ± 1.3
(10,10)	9.3 ± 3.0	1.62 ± 0.35	65.4 ± 1.7	3.35 ± 0.39	78.9 ± 1.4	1.51 ± 0.36	6.5 ± 0.64
(11,11)	3.7 ± 3.2	0.93 ± 0.22	64.1 ± 1.4	2.19 ± 0.21	79.8 ± 1.4	0.81 ± 0.18	3.9 ± 0.35

Note. — Entries in the table are: transition, line velocity and velocity integrated line opacity ($km\,s^{-1}$) for the three velocity components seen in the spectra, and total velocity integrated line opacity. Given the limited signal-to-noise ratio, the line widths of the three components have been fixed at 25.0, 18.8, and 10.6 $km\,s^{-1}$, respectively, as given by the fit to the averaged spectrum of all the transitions observed.

Table 3
H_3O^+ (9,9)/(6,6) Line Ratios and Rotational Temperatures toward Sagittarius B2(N)

Component	V ($km\,s^{-1}$)	$\tau(9,9)/\tau(6,6)$	$T_{\rm rot}$ (K)
Galactic center	–92 to –69	0.59 ± 0.11	467 $(-80, +87)$
Norma arm	–47 to –13	0.69 ± 0.11	556 $(-99, +124)$
Galactic center	–9 to 8	0.66 ± 0.08	524 $(-71, +85)$
Scutum arm	12 to 22	0.69 ± 0.12	552 $(-107, +141)$
Sagittarius B2	47 to 89	0.58 ± 0.04	458 ± 31

Note. — Uncertainties are conservative maximum estimates, allowing a factor of 2 correction due to correlated noise.

describing the population of these high-energy (>400 K above the ground rotational state) metastable levels is uniformly high, in the range 400–700 K (Figure 2; right vertical scale).

The differential rotation of the Milky Way allows, in principle, separating in velocity space spectral features from gas clouds at different galactocentric radii (see, e.g., Vallée 2008, however, the distance determination and hence the assignment to specific spiral arms is complicated due to the streaming motions in the arms, Reid et al. 2009). All velocity components that can be clearly identified in the Sagittarius B2(N) and (M) spectral scan data correspond to the Galactic center gas. There is evidence for broad absorption in the (3,3) and (6,6) lines toward Sagittarius B2(N), but the signal-to-noise ratio is limited. However, H_3O^+ absorption is clearly detected over a broad range of velocities in the deep integrations toward this source (Figure 2). Velocities of the various foreground components on this line of sight are marked with horizontal color bars above the abscissa: green–Galactic center gas, magenta–Norma arm, cyan–Scutum arm, and yellow–Sagittarius arm. Absorption at velocities of the Norma and Scutum arms (magenta and cyan, respectively) is clearly detected, in addition to the Galactic center gas. Averaged optical depth ratios and rotational temperatures for five velocity ranges corresponding to different kinematic components are listed in Table 3.

Determining the uncertainty of the velocity-averaged rotational temperature values is not trivial, as the chan-

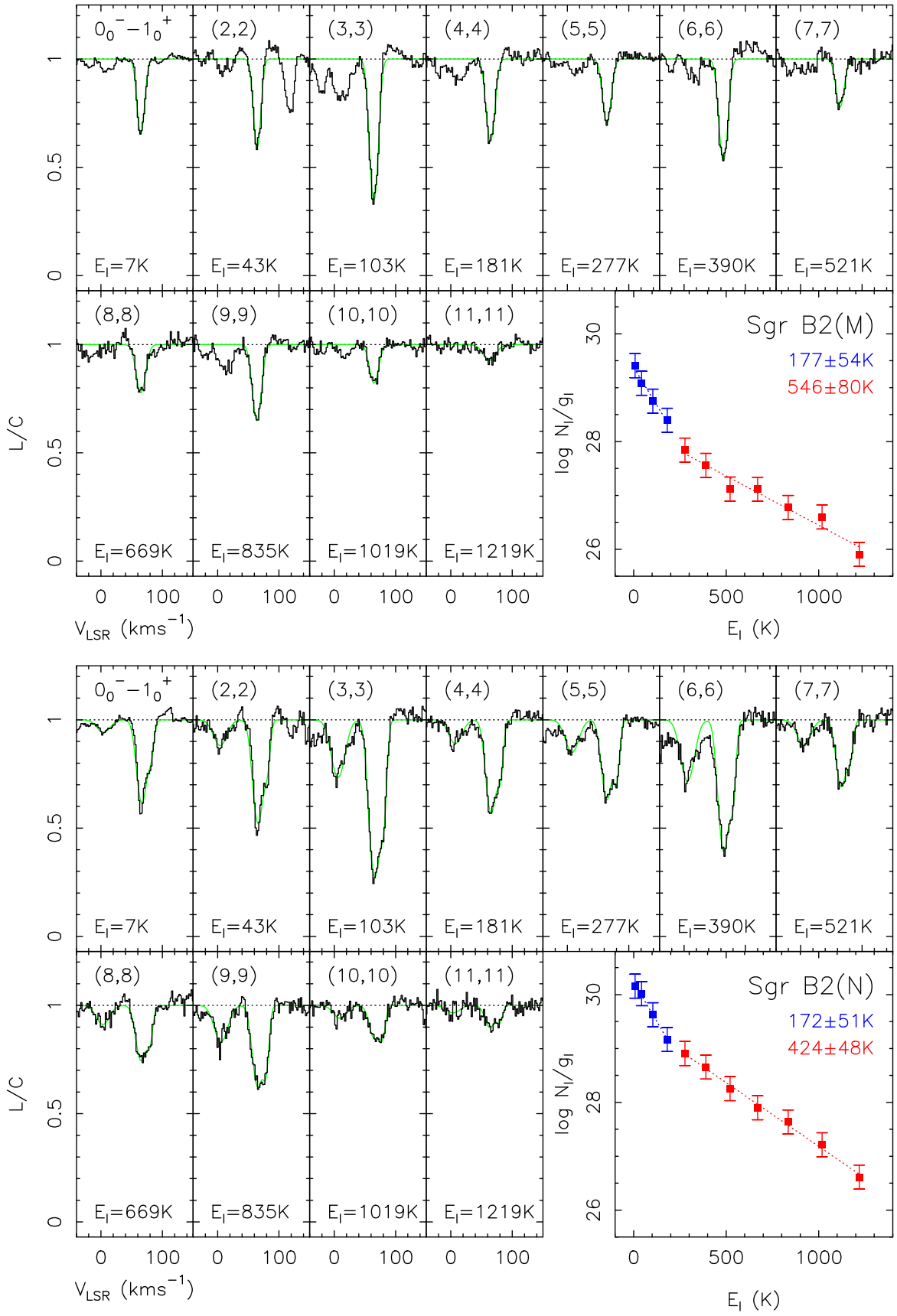

Figure 1. Spectra of the metastable inversion transitions of H_3O^+ toward Sagittarius B2(M) and (N), upper and lower panels, respectively, and the corresponding rotation diagrams. The rotation diagram for Sagittarius B2(M) corresponds to the 64 km s^{-1} component, associated with the cloud envelope, while for Sagittarius B2(N) it corresponds to the sum of the three absorption components seen in the spectra, at ∼5, 65, and 80 km s^{-1}. Green lines are Gaussian fits to the spectra, three components for Sagittarius B2(N) and one component for Sagittarius B2(M). The *maximum* uncertainties of the individual measurements (dominated by systematics) are conservatively assumed to be 25%. The rotational temperatures of the warm and hot components, together with the corresponding maximum uncertainties are listed in the rotation diagram panels.

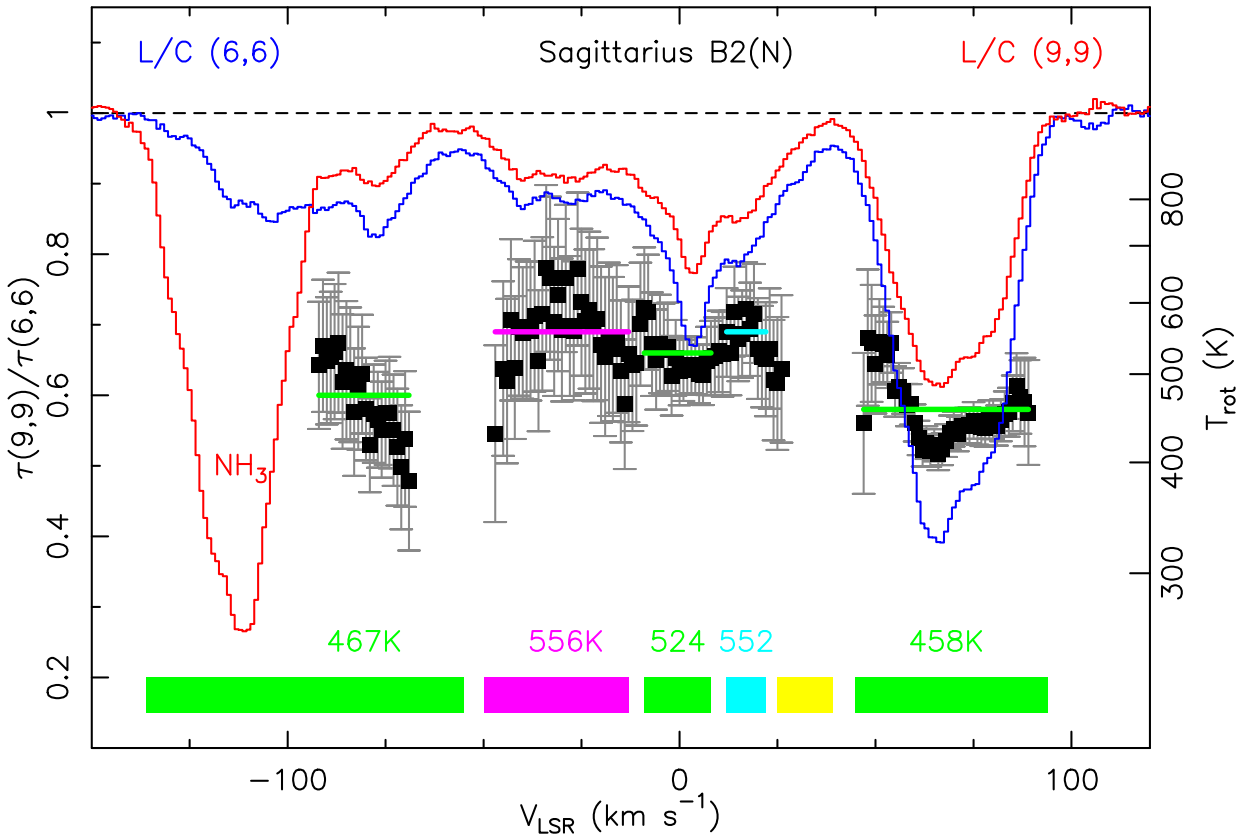

Figure 2. Herschel/HIFI spectra of the (6,6) and (9,9) inversion transitions of the hydronium ion toward Sagittarius B2(N), normalized by the continuum, plotted as a function of the local standard of rest velocity (blue and red lines, respectively). Black points show the (9,9)/(6,6) optical depth ratio with the corresponding 1σ uncertainty in a 1 km s^{-1} velocity bin (left vertical scale). The corresponding rotational temperature scale is shown on the right. Velocities corresponding to the Galactic center material, Norma, Scuttum, and Sagittarius arms are marked in green, magenta, cyan and yellow, respectively, above the horizontal axis (see Table 1).

nels are not independent due to the presence of baseline ripples in the spectra. This aspect has been discussed in detail in the context of the measurements of the water ortho/para ratio by Lis et al. (2013). Based on our previous experience with HIFI HEB data, we allow a factor of 2 correction for the uncertainty of the average line ratio to account for the correlation between the spectral channels. This leads to conservative maximum uncertainties for the line ratio and the rotational temperature listed in Table 3. We conclude that, within the observational uncertainties, the rotational temperature of the hot component is the same, ∼500 K, in regions at different galactocentric distances. As a comparison, the kinetic temperature in the foreground clouds, determined from the NH_3 (1,1) and (2,2) observations, is in the range 10–60 K (Tieftrunk et al. 1994). These low-evergy transitions, however, are not sensitive to the presence of high-temperature gas.

4. W31C RESULTS

Gas motions in the Galactic center region are quite complex, since the velocity field is dominated by the non-axisymmetric bar potential. In particular the gas in the so-called "x2" non-circular orbits may overlap in velocity with the foreground disk clouds. One thus cannot exclude that the H_3O^+ absorption at *all* velocities toward Sagittarius B2 is predominantly associated with the gas in the Central Molecular Zone. The observations of W31C, a line of sight that does not intersect the Galactic center region, provides independent constraints. The (6,6) and (9,9) excited inversion lines of the hydronium ion are also detected in the deep HIFI observations on this line of sight (Figure 3), which samples the diffuse interstellar medium along a 4 kpc line of sight through the Galactic disk. The foreground absorption covers velocities between 10 and 50 km s^{-1} (Gerin et al. 2010; Neufeld et al. 2010), with a strong feature at ∼40 km s^{-1} clearly seen in the H_3O^+ spectra. The observed absorption line intensities are listed in Table 4. The resulting rotational diagram (Figure 4) can again be described by two components with temperatures of 65 K

Table 4
H_3O^+ Absorption Line Strength toward W31C

Transition	τdv
(1,1)	0.30 ± 0.04
$0_0^- - 1_0^+$	0.30 ± 0.04
(2,2)	0.30 ± 0.05
(3,3)	0.40 ± 0.04
(6,6)	0.17 ± 0.02
(9,9)	0.08 ± 0.02

Note. — Entries in the table are: transition and velocity integrated line opacity (km s^{-1}).

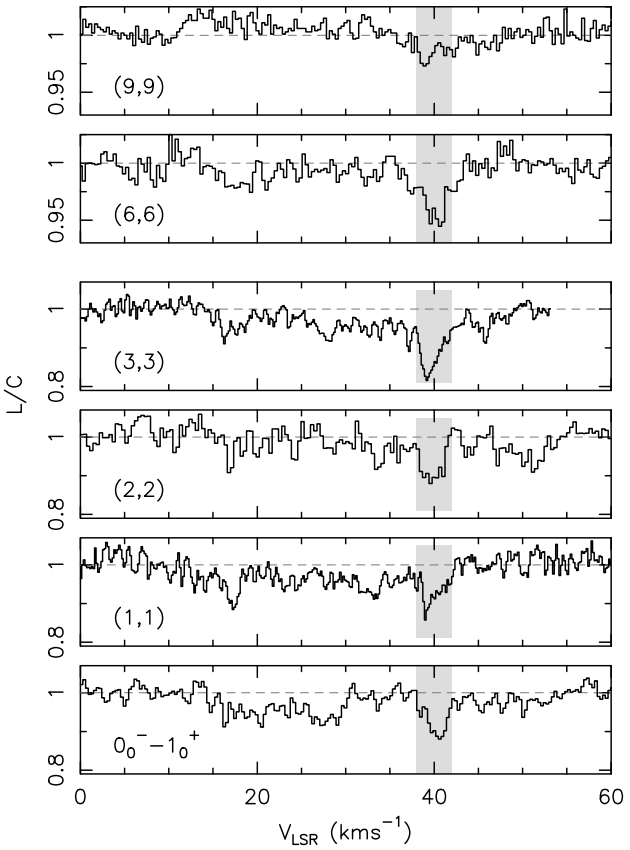

Figure 3. Spectra of the (9,9) and (6,6) inversions transitions of the hydronium ion absorption toward W31C, combined with earlier observations of lower-energy transitions obtained within the PRISMAS GT KP. Weak H_3O^+ absorption is detected at $\sim$40 km s^{-1} (highlighted in light gray). Due to the narrow line width, the (1,1) absorption in this source is not blended with $H_2^{18}O$ and this transition can be used in the analysis. Note that the vertical scale is different for the (6,6) and (9,9) lines.

(+21,–13) K and 380 K (+210,–100) K. The uncertainties are maximum uncertainties, assuming a 35% maximum uncertainty for the individual measurements (a conservative estimate of the combined statistical and systematic uncertainties). Although the uncertainty in the rotational temperature of the hot component is large, the lower bound is well constrained, demonstrating that the population of the excited metastable levels is described by a temperature that is significantly higher than that describing the low-energy metastable rotational levels, in agreement with the Sagittarius B2 results. The 65 K temperature describing the population of the low-energy metastable levels is consistent with the kinetic temperature of the gas in the diffuse interstellar medium in the Galactic disk (Snow & McCall 2006).

From the two-component fit to the rotation diagram, we estimate a total H_3O^+ column density of 1.2×10^{13} cm^{-2} toward W31C, with $\sim$20% in the hot component, as compared to $\sim$40% toward Sagittarius B2(N) and (M).

5. DISCUSSION

Earlier ground-based (Hüttemeister et al. 1995) and space-borne (Ceccarelli et al. 2002) observations of ammonia absorption toward Sagittarius B2 have been interpreted in terms of a physically hot component of molecular gas in the central region of the Galaxy, in which the observed high rotational excitation temperature traces a correspondingly high kinetic temperature. At first glance this seems plausible, because shock waves in this active high-mass star-forming region should be able to maintain some molecular gas at temperatures of 500 to 700 K, or because the region contains luminous heating sources of X-rays and cosmic rays. Moreover, strong X-ray emission in iron fluorescence at 6.4 keV has been taken as evidence that the envelope of Sagittarius B2 was recently illuminated by an X-ray flash, attributable to a flare from the region around the central black hole that is associated with the Sagittarius A* radio continuum source (Sunyaev et al. 1993; Koyama et al. 1996). The Sagittarius B2 X-ray flux is now fading (Terrier et al. 2010), with a characteristic decay time of 8 years, comparable to the light-travel time across the central part of the molecular cloud.

While the competing mechanisms put forward to explain the hot gas component on the line of sight toward Sagittarius B2 are all plausible, a generally accepted explanation has yet to be offered. Interestingly, recent observations of the (8,8) to (15,15) ammonia inversion lines (Mills & Morris 2013) indicate rotational temperatures of 350–450 K in several largely *quiescent* Galactic center giant molecular clouds. This indicates that the effect is not limited to Sagittarius B2, but widespread in the Galactic center environment. The hot gas component traced by the high-energy ammonia inversion lines would thus have to fill a few hundred parsec size region. The energy input required to heat such a vast volume of gas would then have to be carefully evaluated. Moreover, the diffuse, widespread, low-density gas component in the Central Molecular Zone can be independently probed through the infrared absorption spectroscopy of the H_3^+ rovibrational transition (Oka et al. 2005), which indicate temperatures of "only" $\sim$250 K. Inversion lines of ammonia, up to (10,10), have also been detected in absorption toward PKS 1830-211, indicating rotational temperatures $\gtrsim$600 K for the highest-energy lines (Henkel et al. 2008). The absorption is attributed to molecular gas in spiral arms of an ordinary galaxy at a redshift of 0.89.

Explanations similar to those previously invoked to explain the high-rotational temperatures of ammonia cannot easily be applied to H_3O^+: if the density were high enough to thermalize the populations of highly excited rotational states at a kinetic temperature of 400 to 600 K, then molecular collisions would also raise the excitation temperatures of the high-J inversion doublets to values higher than the brightness temperature of the continuum radiation at $\lambda 150 - 200$ μm. In that case, the inversion lines could not appear in absorption as is observed. A fundamentally different interpretation is required to explain simultaneously the high rotational excitation of H_3O^+, its short chemical lifetime, and its relatively large total column density, $N(H_3O^+) = 4{-}7{\times}10^{14}$ cm^{-2}, close to an intense far-infrared continuum source.

The characteristic two-component rotational diagram for metastable states of H_3O^+ naturally results from its formation by exoergic ion-neutral reactions. The excess enthalpy (heat of formation) of the main source reaction

(e.g., Herbst & Klemperer 1973)

$$H_2O^+ + H_2 \rightarrow H_3O^+ + H$$

goes partly into internal rotational excitation of the product ion, the highly excited non-metastable states relax rapidly by spontaneous radiative transitions to the metastable states (i.e. the lower $J = K$ inversion levels), whose populations are limited by the rates of excited-molecule formation and chemical destruction. Populations are partly re-distributed by inelastic collisions and by absorption of the background far-infrared continuum radiation. The populations of the lowest metastable states may approach a collision-dominated thermal distribution. The turnover to a "hot" formation-dominated distribution is detectable when the formation rate is a non-negligible fraction of the inelastic collision rates.

The relation between molecular excitation and formation can be outlined quantitatively as follows. The destruction rate per H_3O^+ molecule by dissociative recombination with electrons can be written $\mathcal{D} = n(e)k_{\rm dr}$ s^{-1}, where the rate coefficient for the process $k_{\rm dr} = 4.3 \times 10^{-7}(T/300)^{-1/2}$ cm^3 s^{-1} at kinetic temperature T (Jensen et al. 2000) and $n(e)$ is the number density of free electrons. At $n(e) \sim 0.01$ to 0.1 cm^{-3}, and $T \sim 50$ to 200 K, $\mathcal{D} \approx 10^{-8}$ to 10^{-7} s^{-1}. This is fast enough to be the dominant destruction mechanism. If we furter assume steady state between destruction and formation, then the formation rate per unit voulme can be written as $\mathcal{F} = n(H_3O^+)\mathcal{D}$ cm^{-3}s^{-1}. With no further knowledge of the chemistry, we can assert that the source of H_3O^+ in the envelope of Sagittarius B2 must be of the order of

$$\mathcal{F} = N(H_3O^+)\mathcal{D}/L \approx 10^{-11}\Big[\frac{1\ {\rm pc}}{L}\Big]\Big[\frac{n(e)}{0.1\ {\rm cm}^{-3}}\Big]\ {\rm cm}^{-3}{\rm s}^{-1},$$

where L is the characteristic length scale of the absorbing region. The interstellar chemistry of oxygen-containing ions is thought to be straightforward (Herbst & Klemperer 1973), with cosmic-ray or X-ray ionizations of hydrogen leading to H^+ and H_3^+, which transfer charge to O^+ or OH^+. The oxygen ions form H_2O^+ and finally H_3O^+ via reactions with H_2. In regions where the atomic fraction is small, $H/H_2 \ll 1$, the chemical source rate of the terminal ion H_3O^+ can be a significant fraction of the hydrogen ionization rate. Thus we can express $\mathcal{F} \sim \zeta n_{\rm H}\epsilon$, where ζ is the ionization rate, $n_{\rm H}$ is the density of hydrogen, and ϵ is a chemical loss factor that accounts for minor channels in the ion chemistry that prevent the hydrogen ions from processing solely the oxygen. Such an analysis has been applied to Herschel/HIFI observations of OH^+ and H_2O^+ in diffuse molecular gas by Neufeld et al. (2010), who concluded that those highly reactive ions arise mostly in components of gas with a high atomic content, unlike H_3O^+, which traces predominantly molecular gas. Following these arguments, we see that the observed column density and estimated destruction rate of H_3O^+ toward Sagittarius B2 require

$$\zeta n_{\rm H} \leq 10^{-11}/\epsilon \quad {\rm cm}^{-3}\ {\rm s}^{-1}\ ,$$

for $L \approx 1$ pc and $n(e) \leq 0.1$ cm^{-1} in the envelope of Sagittarius B2. This could be achieved with a cosmic-ray ionization rate $\zeta \sim 10^{-15}$ s^{-1} at $n_{\rm H}\epsilon \sim 10^4$ cm^{-3}, or with less extreme values if the electron density is lower. Cosmic ray ionization rates in excess of 10^{-15} s^{-1} have been deduced from infrared absorption observations of H_3^+ on several lines of sight through the Central Molecular Zone of the Galaxy (Goto et al. 2013, and references therein).

The line of sight to W31C presents a simpler test case because it lies entirely outside the Central Molecular Zone, where conditions are extreme. For illustration, consider the low-density limit, in which collisional excitation is neglected and the rotational populations are governed entirely by the formation process and radiative transitions. Let the state-specific formation rate of H_3O^+ be described by

$$F(J,K,p) = \mathcal{F}g(J,K,p)\exp\big(-E(J,K,p)/kT_f\big)/Q(T_f)$$

for each state of rotational quantum numbers J, K, and parity p, where g is the statistical weight, $E(J,K,p)$ is the energy, Q is the partition function, and T_f is a parameter—the formation temperature. The populations of the vibration-rotation levels are then computed by solving the rate equations with formation, destruction, and all radiative transitions included (equations 12–15 of van der Tak et al. 2007), but with all the collisional terms set to zero. The results of one example are compared with the observed population diagram in Figure 4. In this case, $\mathcal{D} = 10^{-7}$ s^{-1} (corresponding to $n(e) \approx 0.1$ cm^{-3} at $T < 100$ K) and the total column density is $N(H_3O^+) = 1.4 \times 10^{13}$ cm^{-2}. The formation temperature is $T_f = 400$ K and the molecules are exposed to an average Galactic background continuum similar to that described by Black (1994). At the adopted destruction rate, $\mathcal{F} = 4.5 \times 10^{-14}$ cm^{-3} s^{-1} is required to attain a good match in column density over a total path length $L \approx 10$ pc. This rate, in turn, would imply a rate of cosmic-ray ionization of H_2, $\zeta_2 = \mathcal{F}/n(H_2)\epsilon \approx 5 \times 10^{-16}$ s^{-1} for a density $n(H_2) = 300$ cm^{-2} and $\epsilon \approx 0.3$. This ionization rate would be consistent with that derived by Indriolo et al. (2012) toward W51 IRS2 if the H_3O^+ is found preferentially in regions of higher molecular fraction and higher ϵ than the observed OH^+. These conditions are also in harmony with photochemical models of diffuse molecular gas as discussed by Hollenbach et al. (2012).

A combined excitation-chemistry model, which includes explicitly the exothermicity of the chemical reactions leading to the formation of the hydronium ion and ammonia is beyond the scope of the present paper and will be presented separately (J. Black, in prep.) Such calculations are clearly needed to demonstrate that chemistry and excitation are closely coupled in some interstellar environments and should not be treated separately and to use H_3O^+ as a quantitative tracer of the cosmic ray ionization rate[14]. This aspect is of particular interest for understanding the energetics of the nuclear regions of ultraluminous, star-forming galaxies. Highly-excited inversion lines of the hydronium ion have now been detected in the ultraluminous infrared galaxy Arp 220, as well as in NGC 4418, which harbors a deeply buried, compact AGN (González-Alfonso et al. 2013). In these

[14] One serious impediment is that the collisional cross-sections for H_3O^+ are only available for rotational levels with energies below ~350 K, scaled from ammonia (Offer & van Hemert 1992).

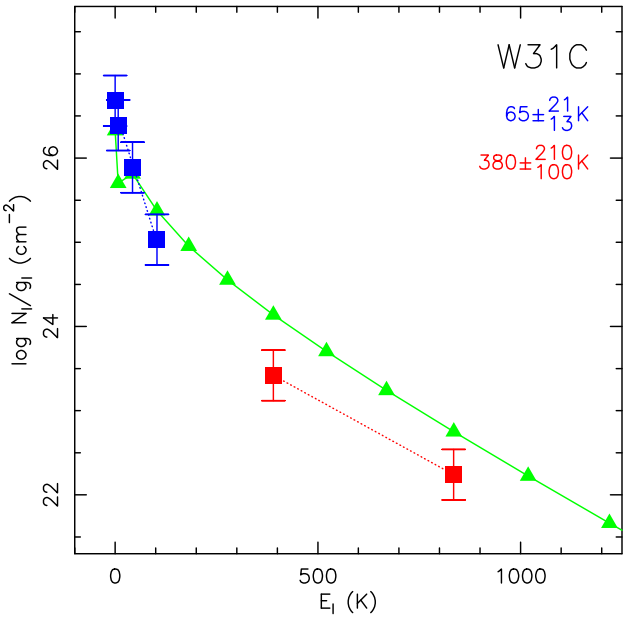

Figure 4. Observed population diagram for H_3O^+ toward W31C (blue and red squares). Derived rotational temperatures of the warm and hot component are given together with the corresponding maximum uncertainties, computed assuming 35% maximum uncertainties of the individual measurement. Green triangles show the H_3O^+ population of the metastable levels computed using the simple formation model described in the text. The model is included for illustrative purposes only and is not meant to be a fit to the data.

environments, the hydronium ion absorption traces a relatively low-density molecular gas with a large filling factor, which is directly influenced by the feedback process of the central engine.

The traditional explanation for these observations invokes a new phase of the interstellar medium, which would have to be heated by some combinations of X-rays, cosmic rays, shocks, or turbulence to ∼500 K. If the chemical formation pumping explanation is correct, this additional energy input is not required—the observations can simply be explained by chemical formation pumping in a much lower temperature medium. This relaxes the heating requirements and simplifies the physical picture of the interstellar medium in these active environments. With the improved understanding of the excitation, the far-infrared inversion lines of the hydronium ion also provide an accurate measurement of the ionization rate in the mostly molecular gas component of high-redshift galaxies, using ALMA, highly complementary to the OH^+ and H_2O^+ observations that primarily trace atomic gas, with low molecular fraction (Gerin et al. 2010; Neufeld et al. 2010).

Symmetric top molecules have been proven to be some of the best tracers of the gas kinetic temperature in the interstellar medium (Ho & Townes 1983; Mangum et al. 2013). However, the results presented here suggest that they may sometimes fail as an interstellar thermometer, under specific conditions. This typically involves low-density, diffuse gas, as collisions and strong radiation field tend to drive the rotational level population to equilibrium conditions. Consequently, care has to be taken when interpreting the derived rotational temperatures as physical temperatures of the medium.

HIFI has been designed and built by a consortium of institutes and university departments from across Europe, Canada and the United States (NASA) under the leadership of SRON, Netherlands Institute for Space Research, Groningen, The Netherlands, and with major contributions from Germany, France and the US. Support for this work was provided by NASA (*Herschel* OT funding) through an award issued by JPL/Caltech. The research of PS, CC, and RH is supported by the Collaborative Research Center 956 funded by the Deutsche Forschungsgemeinschaft (DFG).

REFERENCES

Bates, D.R., & Spitzer, L. 1951, ApJ, 113, 441
Black, J. H. 1994, The First Symposium on the Infrared Cirrus and Diffuse Interstellar Clouds. ASP Conference Series, Vol. 58, R.M. Cutri and W.B. Latter, Eds., p.355
Bergin, E. A., Phillips, T. G., Comito, C., et al. 2010, A&A,
Cheung, A. C., Rank, D. M., Townes, C. H., et al. 1969, Natur, 221, 626
Ceccarelli, C., Baluteau, J.-P., Walmsley, M., et al. 2002, A&A, 383, 603
Comito, C., & Schilke, P. 2002, A&A, 395, 357
De Graauw, Th., Helmich, F. P., Phillips, T. G., et al. 2010, A&A, 518, L6
Evans, N.J. II. 1999, ARA&A, 37, 311
Flower, D. 2007, Molecular Collisions in the Interstellar Medium, 2nd Edition (New York: Cambridge University Press)
Flower, D. R., Pineau des Forêts, G., & Walmsley, C. M. 1995, A&A, 294, 815
Gerin, M., de Luca, M., Black, J., et al., A&A, 518, L110
Goldsmith, P. F., & Langer, 1978 ApJ, 222, 881
González-Alfonso, E., Fischer, J., Bruderer, S., et al. 2013, A&A, 550, A25
Goto, M., Indriolo, N., Geballe, T. R., & Usuda, T. 2013, JPCA, 117, 9919
Habart, E., Walmsley, M., Verstraete, L., et al. 2005, SSR, 119, 71
Henkel, C., Brratz, J. A., Menten, K. M., & Ott, J. 2008, A&A, 485, 451
Herbst, E., & Klemperer, W. The 1973, ApJ, 185, 505
Higgins, R. D., & Kooi, J. W. 2009, Proc. SPIE, 7251, 72150L
Ho, P. T. P., & Townes, C. H. 1983, ARA&A, 21, 239
Hollenbach, D., Kaufman, M. J., Neufeld, D., Wolfire, M., & Goicoechea, J. R. 2012, ApJ, 754, 105
Hüttemeister, S., Wilson, T. L., Mauersberger, R., et al. 1995, A&A, 294, 667
Indriolo, N., Neufeld, D. A., Gerin, M., et al. 2012, ApJ, 758, A83
Jensen, M. J., Bilodeau, R. C., Safvan, C. P., et al. 2000, ApJ, 543, 764
Koyama, K., Maeda, Y., Sonobe, T., et al. 1996, PASJ, 48, 249
Linke, R.A., Frerking, M.A., & Thaddeus, P. 1979, ApJ, 24, L139
Lis, D. C., Schilke, P., Bergin, E. A., et al. 2012, RSPTA, 370, 5162
Lis, D. C., Bergin, E. A., Schilke, P., & van Dishoeck, E. F. 2013, JPCA., 117, 9661
Liu, D.-J., & Oka, T. 1985, PhRvL, 54, 1787
Mangum, J. G., Darling, J., Henkel, C., et al. 2013, ApJ, 779, 23
McKellar, A. 1940, PASP, 52, 187
Mills, E. A C., & Morris, M. R. 2013, ApJ, 772, 105
Neufeld, D. A., Sonnentrucker, P., Phillips, T. G., et al. 2010, A&A, 518, L108
Offer, A. R., & van Hemert, M. C. 1992, CP, 163, 83
Oka, T., et al. 2005, ApJ, 632, 882
Pilbratt, G. L., Riedinger, J. R., Passvogel, T., et al. 2010, A&A, 518, L1
Reid, M. J., Menten, K. M., Zheng, X. W., Brunthaler, A., & Xu, Y. 2009, ApJ 705, 1548
Roelfsema, P. R., Helmich, F. P., Teyssier, D., et al. 2012, A&A, 537, A17
Snow, T. P., & McCall, B. J. 2006, ARA&A, 44, 367
Solomon, P. M. & Vanden Bout, P. A. 2005, ARA&A, 43, 677
Sunyaev, R. A., Markevitch, M., & Pavlinsky, M. 1993, ApJ, 407, 606
Swings, P., & Rosenfeld, L. 1937, ApJ, 86, 483
Terrier, R., Ponti, G., Bélanger, G., et al. 2010, ApJ, 719, 143
Tieftrunk, A, Pineau des Forêts, Schilke, P., & Walmsley, C. M. 1994, A&A, 289, 579
Vallée, J. P. 2008, AJ, 135, 1301
van der Tak, F. F. S., Black, J. H., Schöier, F. L., Jansen, D. J., van Dishoeck, E. F. 2007, A&A, 468, 627
Weinreb, S., Barrett, A. H., Meeks, M. L., & Henry, J. C. 1963, Natur, 200, 829

Wilson, R. W., Jefferts, K. B., & Penzias, A. A. 1970, ApJ, 161, L43
Yu, S., & Pearson, J. C. 2014, ApJ, submitted